Accepted for publication in *Composites Part A*, 2020

Unification and parameterisation of 2D and 3D weaves and the formulation of a unit cell for composites made of such preforms

Mingming Xu[1], Elena Sitnikova[1*], and Shuguang Li[1]
[1]Faculty of Engineering, University of Nottingham, Nottingham NG8 1BB, UK
*Corresponding author (elena.sitnikova@nottingham.ac.uk)

Abstract

In this paper, the method to unify the definition of woven architectures in textile composites over a wide range of variations has been established. This was achieved via parametrisation of the weaves, which was conducted employing a limited set of clearly defined parameters. Detailed description of these parameters has been given, based of which a wide range of 2D and 3D weaves can be reproduced. The intended use of the parametrisation developed is to facilitate virtual testing of composites through numerical material characterisation based on use of unit cells (UC). The process as presented in this paper delivers a fully parametrised UC in a straightforward way. After implementing the parametrisation as a computer code and combining it with the piece of software UnitCells©, it has been fully developed as a methodology. Its capability as a design tool for 3D woven composites is demonstrated via a range of case studies.

Keywords

A. Fabrics/textiles; B. Mechanical properties; C. Micro-mechanics; Parametrisation.

1 Introduction

The potential of 3D woven textile composites in engineering applications has fascinated designers of composite materials and structures for a long time. They offer exactly what conventional laminated composites are short of, namely, the integrity in the thickness

direction and hence the improved transverse performance [1]. However, in order to take full advantage of textile composites in structural applications, there should be reliable and affordable means of assessing their performances, without which their mere acceptance in engineering as serious candidates for structural materials is unthinkable. Their characterisation through purely experimental means proves impractical because there are too many design variables involved in the architecture of 3D textile preforms to explore.

Conventional method of characterising materials in engineering is through their mechanical testing on coupons according to relevant standards, where their properties are obtained, and there have been a substantial number of research papers reporting the efforts in this direction for 3D woven textile composites [2-6]. Studies of this kind typically investigate the effect of specific preform architectures or geometric parameters of the weave on the mechanical performance of the composite. However, because of the abundance of geometric parameters of the weaves, to obtain by such means a knowledge base of any practical value for designers is apparently untenable. Sometimes, small changes in design variables could mean rather different fabrication process for some the woven textile preforms. For instance, in woven textile preforms, the tows are oriented in two mutually orthogonal directions, warp and weft. Fibre orientations are typical design variables for designers of composites structures. A completely different manufacturing process would have to be employed in this case if one wished to change the orientation for any of the fibre tows. The experimental 'trial and error' approach is therefore not a viable route for textile composites to gain wide acceptance in engineering.

Virtual testing, on the other hand, can offer a way forward in this respect. Typically, numerical characterisation of textile composites is conducted via multiscale modelling, which heavily relies on use of unit cells (UCs). Once again, there is a substantial volume of publications addressing UC modelling of 3D textile composites [7-10]. However, the UC modelling has not yet become accepted as an engineering design tool in industry due to the lack of comprehensive and verified methodology for the UC analysis as a practical design

tool in general. This is undoubtedly the bottleneck on the virtual testing side, which hinders the establishment of the capability for systematic characterisation of 3D textile composites.

The variety of types of the weaves poses a serious obstacle in applications of textile composites, since it makes the selection of the type of the weave best suited for a specific application a truly overwhelming task. Furthermore, lack of systematic definition of 3D weaves that would allow straightforward differentiation between different types of them [11] certainly does not add clarity in this respect. In the literature, a variety of methods for defining the geometry of 3D interlock textiles have been proposed [11-13]. Some classify weave types based on fabrication process considerations and interlacing position of warp tows [7], based on which a range of parameters are identified for describing the weave [11].

The problem of selection of the weave type for a specific application can be made more manageable if the definition of architecture and the topology of various weave types were unified so that it would be described via a limited set of parameters. Such parametrisation of the textile composites will be the first objective of this paper. It is worth noting that the parametrisation established is intended mainly for composite designers dealing with the mechanical behaviour of these material. The preform manufacturers can have their own terminology and use their own tools, such weave diagrams, etc. To bridge the gap between successful practical applications of these composites and technologies available to make sophisticated 3D textile fabrics, a dialogue must be established between the designers and the manufacturers. Authors hope that the method as established in the paper can help forming a platform for such a dialogue.

The method takes advantage of the translational symmetry present in the architecture of weaves due to the relatively accurate control of the tow position in the fabrication process of modern textile preforms. The considerations apply equally to 2D and 3D weaves. The key advantage of the proposed parametrisation method is that the process can be transferred to the formulation of UCs for composites made of such preforms. A fully parametrised UC for woven textile composites, unified between 2D and 3D weaves and weaves of different interlacing architectures, will be rigorously formulated in this paper. Its implementation as a

computer code, also presented in the paper, has been highly automated, delivering a much needed capability which can be exploited as a practical design tool for woven textile composites.

2 Parameterisation of the woven textile

In contract to approaches commonly employed in the literature, where the UCs for woven composites are defined based on translational symmetries along orthogonal directions, e.g. [7, 14-17], those along non-orthogonal directions will be explored here. All weaves can be viewed as a stack of slices along the weft direction, with each slice containing only one set of warp tows. If one of them, referred to as base slice as indicated by the hatched strip in Fig. 1, is taken as the original, other slices can be considered as its images, reproduced through a certain translational symmetry [18], as depicted in Fig. 1 as a plan view of the fabric. Within the base slice, periodicity can usually be identified, e.g. the shaded part as in Fig. 1, which will lead to appropriate definition of the UC. The UC so introduced is expected to be more efficient than those resulting from translations along orthogonal directions.

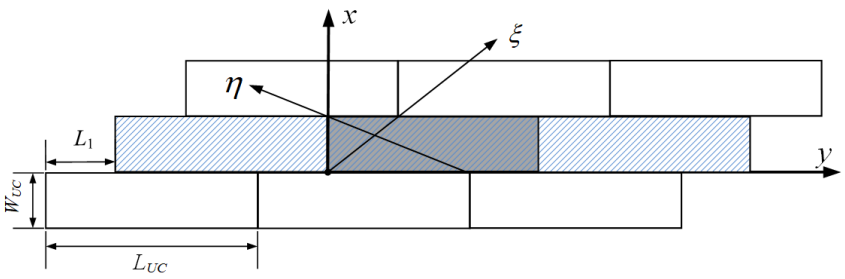

Fig. 1 Translational symmetry along non-orthogonal directions in the *xy*-plane

If the slices were lined up with one another, with one of them being taken as the base slice while the rest the images of the base slice under translational symmetries along the weft direction, i.e. in an orthogonal manner, one would obtain a collection of loose tows in weft and warp directions respectively without any interlocking. A simple example to illustrate this is presented in Fig. 2(a) where two such slices are shown. The view of Fig. 2(a) is slightly

slanted so that two slices can be visualised. There are two sets of warp tows, one highlighted in blue and another in pink. The weft tows, cross-sections of which are shown as circles, are regularly arranged in the vertical and in the horizontal direction to form an array. Interlocking takes place when the slice at the back (with pink warp tows) is shifted horizontally relative to that in the front (with blue warp tows) by a full spacing between the weft tows, and the weft tows are re-aligned and re-joined, as shown Fig. 2(b). With multiple slices involved, the interlocking can be viewed more clearly and realistically as illustrated in Fig. 2(c).

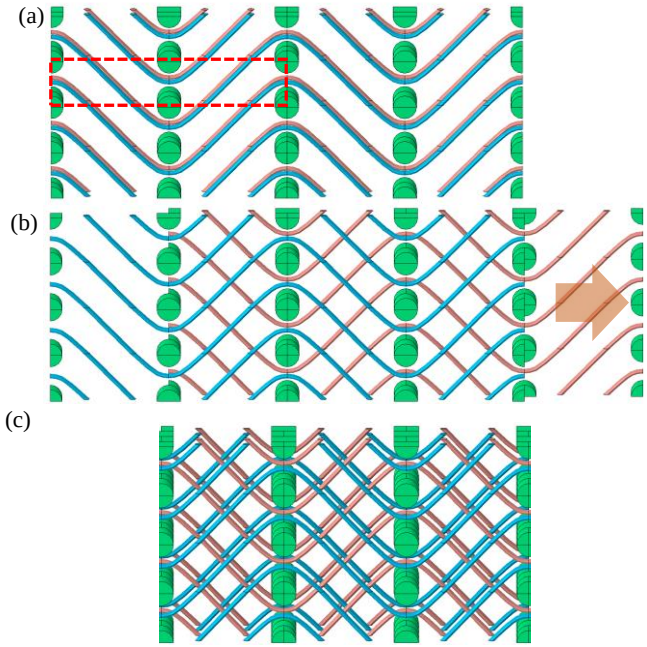

Fig. 2 Schematic view of the interlocking: (a) two aligned slices; (b) slices after shifting and (c) four slices illustrating full interlocking as a result of shifting

With the shifted slice being viewed as an image of the base slice, the symmetry transformation can be described as combination of the translation into the page orthogonally and another corresponding to the shift. The combined effect is a translation along direction ξ as illustrated in Fig. 1, which is apparently non-orthogonal. With the help of this translation, all slices in an interlocked fabric can be reproduced from a base slice. It is therefore sufficient to parametrise the topology of the slice before the complete weave can be appropriately described.

It is worth noting certain features that are not uncommon in 3D weaves, such as stuffer warp tows, or additional warp tows on surfaces of the fabric, are not reflected in this study. The parametrisation can be extended in a reasonably straightforward way to accommodate some of these features, such as stuffer tows. However, to avoid deviating from the focus of this paper, this has been omitted. Practical 3D fabrics tend to have surface tow interlacing pattern different from that in the interior over the thickness. This is not addressed in this paper either because the periodicity in 3D space has been assumed.

2.1 Topological parameters of woven architectures

To describe the topology of the base slice, five integer parameters are identified that are found to be sufficient for the task. This stage of parametrisation is largely descriptive, involving some simple visualisation of the geometry, hence the full set of these parameters is listed in Table 1, where their functions are elaborated and the ranges of values they can be prescribed are specified.

Table 1 Topological parameters of the weave

Notation	Meaning	Values taken
n_{offset}	a switch indicating variation in the weave patterns of weft tows inside a slice	0: no offset, as in Fig. 2 1: horizontal offset, as in Fig. 3(a) -1: vertical offset, as in Fig. 3(b)
n_{skip}	the number of weft tows the warp tow skips before turning	1: immediate turn, as in Fig. 2(a) and Fig. 4(a) k>1: turn after skipping k weft tows, as in Fig. 4(a) for k=2
n_{deep}	the number of rows of the weft tows a warp tow moves past through the thickness before making a turn	0: warp tow remains flat 1: corresponds to 2D weaves k>1: 3D weaves
n_{steep}	the number of rows of the weft tows a warp tow passes by before crossing a column of the weft tows	0: warp tow remains flat 1: 2D or 3D weave 1<k< n_{deep}: 3D weave
n_{step}	topological descriptor indicating the resulting dislocation of each slice in terms of the number of columns of the weft tows	0: no shift, as in Fig. 2(a) 1: shift by one column of weft tows, as in Fig. 2(b) and (c) k>1[a]: relevant for sophisticated woven architectures

[a] the value should be less than the number of columns of weft tows in a full period in the direction of shifting

Note that the parametrisation of topology does not require explicit definition of the weave in terms of number of warp or weft tows. Those are determined automatically once the topological parameters of the weave as specified in Table 1 are defined. In real fabric preforms for structural parts, there may be some variation in shape of preform, e.g. varying thickness, at different locations in the part, and hence the number of weft tows may not be constant. However, the variation of the textile pattern is beyond the scope of this study, because the use of a unit cells as adopted in the present work is based on the assumption of periodicity in the pattern.

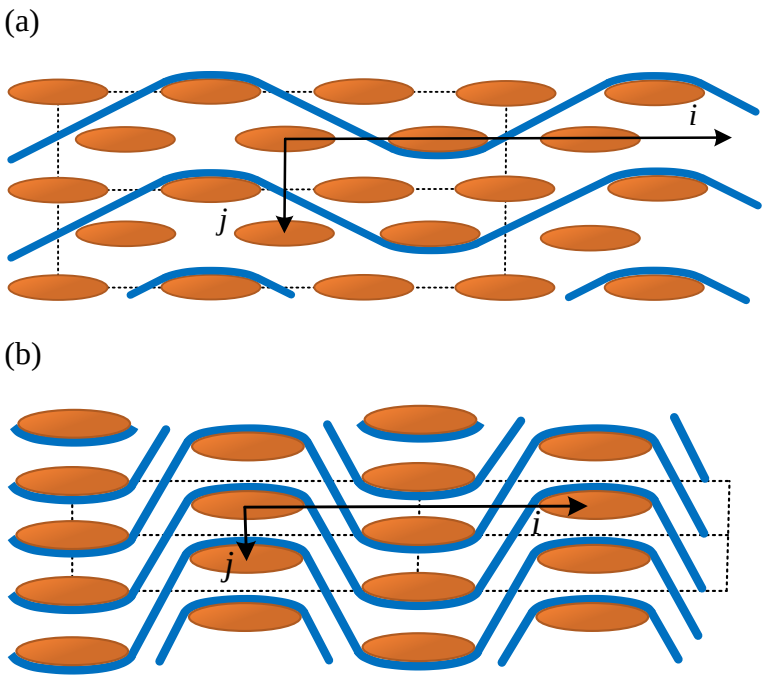

Fig. 3 Offset of (a) the rows of the weft tows in the horizontal direction and (b) the columns of the weft tows in the vertical direction

With the five topological parameters as introduced in Table 1, the topology of a 3D weave can be defined with a reasonably wide coverage for most regular weave patterns of practical significance, whilst having the scope of being extended. One example of such extension is the

definition of parameter n_{skip}. Its definition as presented in Table 1 suggests that the warp tow skips the same number of tows when turning upwards or downwards. To allow for describing certain weave types, such as the satin weave, this parameter can be defined such that it assumes different values on upwards and downward movement of the tow, respectively.

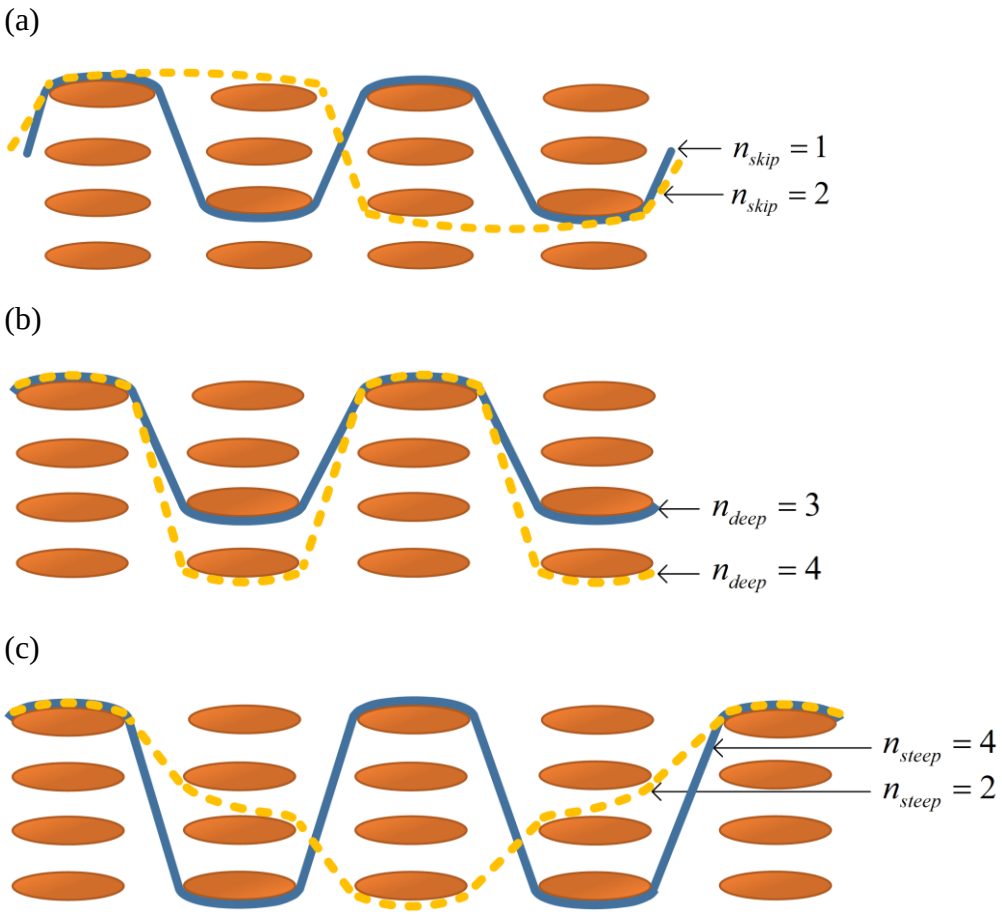

Fig. 4 Illustration of the topological parameters specifying the undulation of the warp tows (a) n_{skip}, (b) n_{deep} and (c) n_{steep}

To demonstrate the use of these parameters in the definition of the topology of woven textile preforms, several typical weave architectures have been associated with the values or ranges of these parameters in Table 2. In each case, the topology of any particular weave has been defined as a combination of five parameters introduced above. Two 3D weaves, one from each category of the two included in Table 2, have been plotted in Fig. 5(a) and Fig. 5(b).

The topology of 2D weaves can also be generated in the same manner, although the actual generation of 2D weaves also requires a slight extension in the geometric aspect as will be further discussed later.

Table 2 Parametrisation of weaves using five topological parameters

Type of the weave	Architecture of the weave	Topological parameters		
		n_{deep} & n_{steep}	n_{skip}	n_{step}
2D weave	Plain	$n_{deep} = n_{steep} = 1$	$n_{skip} = 1$	$n_{step} = 1$
	Twill	$n_{deep} = n_{steep} = 1$	$n_{skip} \geq 2$	$n_{step} = 1$
	Satin	$n_{deep} = n_{steep} = 1$	$n_{skip\_up} \geq 2$ $n_{skip\_down} = 1$	$n_{step} = 1$
3D weave	Angle interlock ($n_{offset} = 0$)	$n_{deep} \geq 2$ $n_{deep} \geq n_{steep} \geq 1$	$n_{skip} \geq 1$	$n_{step} \geq 1$
	Offset interlock ($n_{offset} = \pm 1$)	$n_{deep} \geq 2$ $n_{deep} \geq n_{steep} \geq 1$	$n_{skip} \geq 1$	$n_{step} \geq 1$

2.2 Parametrisation of fibre tow cross-section

With the architecture of the weave being parametrised, the same can be done for the geometry of the fibre tows. When modelling the fibre tows, one of the most important considerations is to reproduce the practical fibre volume fraction whilst avoiding the interference of the neighbouring tows, which is a commonly encountered issue in modelling the textiles. This can be challenging, as in reality, fibre tows in textile composites tend to adapt their cross-sections locally along their length to leave room for other tows whilst filling up the vacant spaces, thus minimising the matrix contents. Simulating such variation in cross-section geometry is a demanding exercise, which is rarely attempted [8], and will not be pursued in this paper either. Tow cross-sections will therefore be assumed to remain constant along their length, whilst the shapes and areas of tow cross-sections for warp and weft tows are allowed to be different from each other. The tow geometry parameterisation as presented below is capable of achieving the tow volume fraction of 70% in most cases for a wide range

of 3D preforms. Assuming a reasonable fibre volume fraction of 70% in tows, it would result in an overall fibre volume fraction of about 50%, which should be pretty much what 3D woven composites could realistically reach. The intricacies of the fibre tow geometry, such as variations of their cross-section along the tow path, do not have a significant effect on the predictions of the effective elastic properties. Because of this, as long as the parametrisation allows reproducing realistic fibre and tow volume fractions, it can be considered adequate for the present purpose.

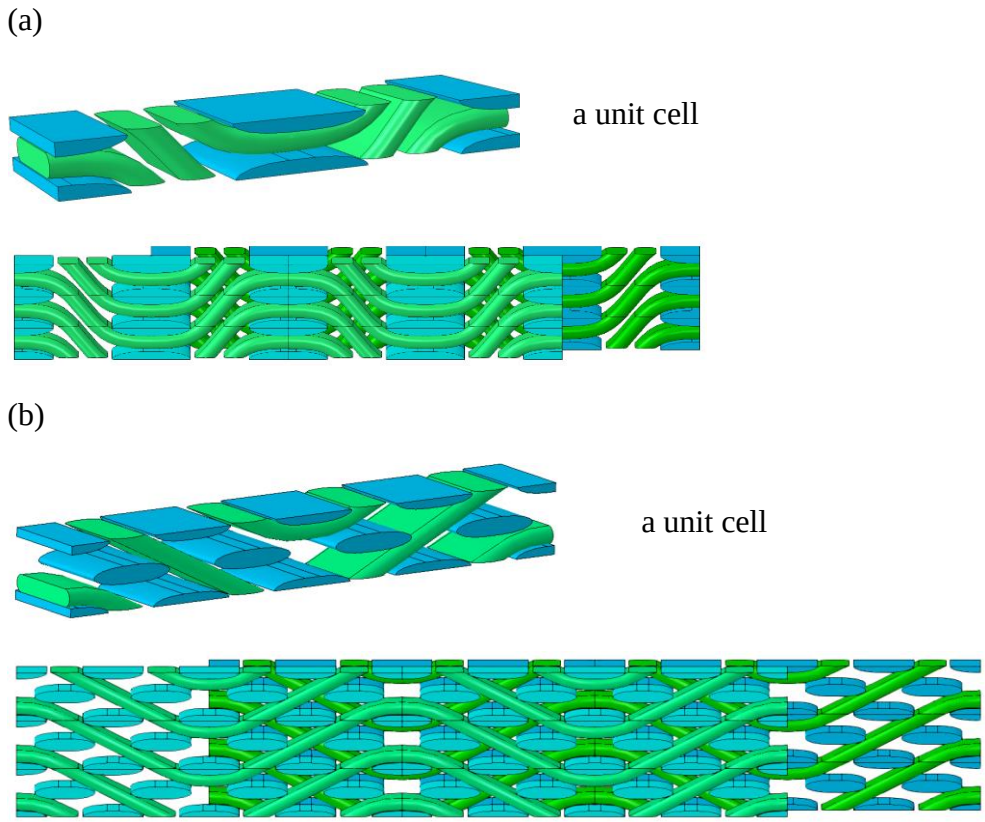

Fig. 5 Typical 3D woven preform architectures as defined by the topological parameters (a) ply-to-ply interlock (n_{offset}=0, n_{step}=1, n_{skip}=1, n_{deep}=2, n_{steep}=2) and (b) offset interlock (n_{offset}=1, n_{step}=2, n_{skip}=1, n_{deep}=3, n_{steep}=3)

According to the microscopic observations [2, 3, 19, 20], the shape of the cross-sections of fibre tows in 3D woven composites varies mostly between an ellipse and a rectangle. Specifically, due to the interlocking mechanism, warp tows cross each other at a regular spacing and hence are periodically constrained on their sides by neighbouring warp tows, whilst the presence of weft tows above and below keeps them in their positions. This biaxial

compaction tends to shape the cross-section of warp tows so that resembles a rectangle with rounded corners. For weft tows, the pressure on the top and bottom transmitted through the neighbouring layers above and below, or compaction applied by the tool during the forming process of the composite, tends to flatten to top and bottom surfaces of their cross-sections. Towards the sides, weft tows tend to conform to the undulating warp tow paths. As a compromise of all these considerations, the tow cross-section is assumed to take a shape of an ellipse split in the middle and filled with a rectangle, as shown in Fig. 6.

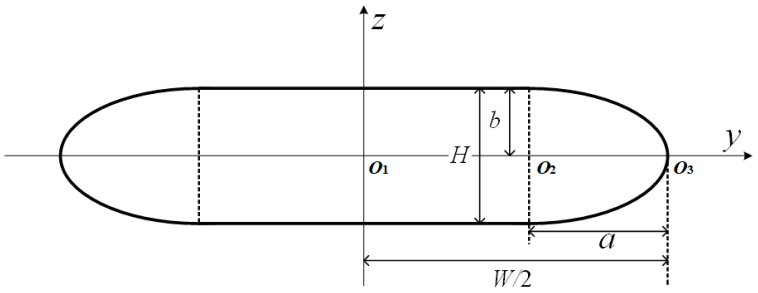

Fig. 6 The assumed fibre tow cross-section as an assembly of a rectangle and two semi-ellipses, one at each end of the rectangle

The elliptical profile on both sides is expected to offer the rounded corners for the warp tows as well as the curvature required for weft tows to conform to the surrounding warp tows. The ellipse can be described by the horizontal and vertical semi-axes, a and $b = H/2$, where H is the height of the rectangle. At a given b, the horizontal semi-axis a determines the actual shape of the ellipse, or the roundness of the corners of the tow cross-section profile. To quantify this effect, another geometric parameter of cross-section, γ, is introduced as the ratio of the width of the elliptical part to the full width of cross-section, W, as follows:

$$\gamma = \frac{2a}{W}. \tag{1}$$

In the actual weaves, the tows tend to have a flattened appearance. Therefore, it is reasonable to restrict the aspect ratio of the tow cross-sections, as given by Eq. (1), such that $W \geq H$. Equality $W=H$ represents a special case where the tow cross-section is either circular (when $a=H/2$) or square (when $a=0$), whilst at any $W \geq H$ the tow cross-section width is larger than its height. Given the construction of the cross-section as introduced in Fig. 6, the range of γ has to be $0 \leq \gamma \leq 1$. Over this range, the cross-section varies from a

rectangle to an ellipse. Additionally, γ can also be prescribed a value of 2 outside its definition in Eq. (1) to signify a special arrangement of a lenticular cross-section section which is often defined for weft tows as they are wrapped by undulating warp tows. A number of special cases corresponding to different values of γ are listed in Table 3 associated with their specific geometric characteristics along with a graphic representation shown in Fig. 7.

Table 3 Tow cross-section parameter ranges

Parameter values/ranges	Shape of cross-section
$\gamma = 0$	a rectangle (a square if W=H)
$H/W > \gamma > 0$	a rectangle with semi-elliptical ends (major axis being vertical and hence lightly rounded ends);
$\gamma = H/W$ (implying a=b)	a rectangle with semi-circular ends or a circle if W=H
$1 > \gamma > H/W$	a rectangle with semi-elliptical ends (major axis being horizontal and hence large chamfers)
$\gamma = 1$	an ellipse (a circle if W=H)
$\gamma = 2$	a lenticle

To allow for different shapes of cross-sections of warp and weft fibre tows, they can be defined with two different sets of geometric parameters, denoted as H_a, W_a, γ_a and H_b, W_b and γ_b, respectively.

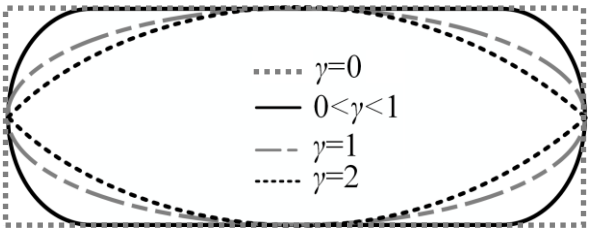

Fig. 7 Typical tow cross-section profiles as specified by the shape parameter γ

2.3 Parametrisation of fibre tow path

To complete the parametrisation of the weave, a set of parameters should be identified that define the warp tow path. It is assumed that a warp tow conforms with the profile of the weft tow as it turns around a weft tow. Before the turn, it follows a horizontal straight line, although the length of this stretch of path could be zero if $\gamma = n_{skip}=1$. After the turn, it follows an inclined line, to proceed to the next column of weft tows. A complete period of the warp tow path can be described as follows.

It is divided into a number of symmetric segments. As a special case, for the weave as shown in Fig. 8 the number of such segments is four. Taking the segment *OSTR* as the original, segment *O'S'T'R'* can be generated by a 180° rotation about point *R*. Applying a reflectional symmetry about the *xz*-plane, the remaining two segments on the left are reproduced. Depending on the actual location of the warp tow within a UC, the order of the four segments within a complete period can be rearranged to reflect the phase difference between different warp tows.

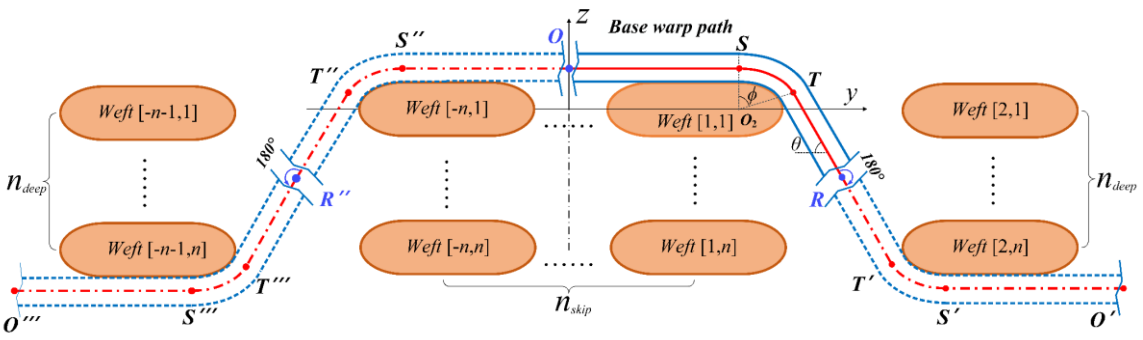

Fig. 8 A complete period of the warp tow

Since, as was stated earlier, the variability of tow cross-section has not been considered, the top and bottom surfaces of the warp tow remain parallel throughout its entire length, including the stretch around the turn. Inference between the adjacent warp and the weft tows is prevented by assuming that the warp tow stays in contact with the weft tow until it straightens as it leaves the weft tow, as shown in magnified and elaborated view of the *OSTR* segment sketched in Fig. 9.

The segment *OSTR*, as shown in Fig. 8 and Fig. 9, can be divided into three sub-segments, *OS*, *ST* and *TR*. Sub-segment *OS* starts from the centre as a horizontal straight stretch resting on top of the row of weft tows. Its length, L_{OS}, is expressed as

$$L_{OS} = \frac{1}{2}\left[\left(n_{skip}-1\right)\left(W_b+D_b\right)+\left(1-\gamma_b\right)W_b\right] = \frac{1}{2}\left[\left(n_{skip}-\gamma_b\right)W_b+\left(n_{skip}-1\right)D_b\right] \tag{2}$$

Sub-segment *OS* is followed by a curved sub-segment *ST* which wraps around the elliptical weft tow. It then turns back to a straight sub-segment *TR* inclined at an angle of θ, which is as interlocking angle of the warp tow as can be seen in Fig. 9.

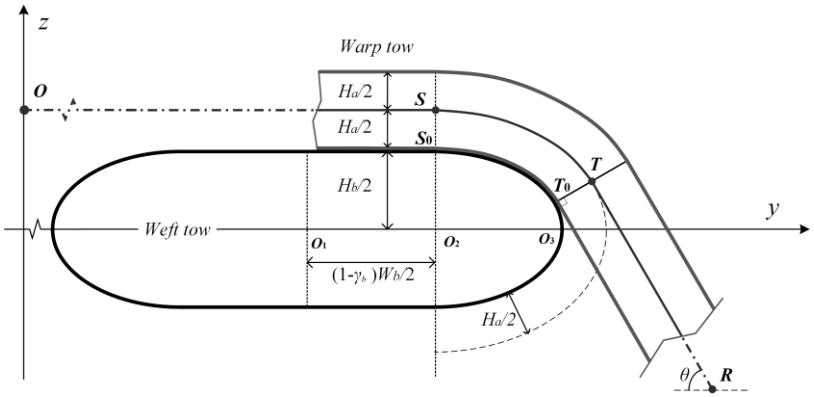

Fig. 9 A typical segment of the warp tow path in relation to the interacting weft tow

To facilitate the definition of the warp tow path, parametric expressions for curves representing different segments have been derived as follows.

Segment *OS* is a straight line defined as

$$z = \frac{1}{2}\left(H_a + H_b\right), \qquad y \in \left[0, L_{OS}\right] \tag{3}$$

Sub-segment *ST* is a parallel curve [21] to the elliptical weft tow profile. The semi-ellipse as the weft tow profile is expressed in its parametric form as

$$\begin{aligned} y &= a\cos(\varphi)+L_{OS} \\ z &= b\sin(\varphi) \end{aligned} \qquad \varphi \in \left[-\frac{\pi}{2}, \ \frac{\pi}{2}\right] \tag{4}$$

where $a = \gamma W_b/2$ is the horizontal semi-axis and $b = H_b/2$ is the vertical semi-axis.

The curve parallel to the ellipse by a distance of $H_a/2$ outside of the ellipse can be obtained as [21]:

$$\begin{aligned} y &= \left(a + \frac{bH_a}{2r} \right) \cos(\varphi) + L_{OS}, \\ z &= \left(b + \frac{aH_a}{2r} \right) \sin(\varphi), \end{aligned} \qquad \varphi \in \left[\varphi_0, \quad \frac{\pi}{2} \right] \tag{5}$$

where $r = \sqrt{a^2 \sin^2(\varphi) + b^2 \cos^2(\varphi)}$.

It should be stressed that φ is a parameter in the parametric form of definition of the ellipse, not the angular polar coordinate at a point corresponding to φ as defined by (5). Since the centre line of the warp tow over the segment *ST* is parallel to the elliptical profile of the weft tow, the respective tangential points, *T* and T_0, where the inner surface of the warp tow departs from the surface of the elliptical weft tow profile correspond to the same value φ_0 of parameter φ. The slopes of their tangents at $\varphi=\varphi_0$ are identical and also equal to the slope of sub-segment *TR*, therefore

$$\tan(\theta) = -\left(\frac{dz}{dy} \right)\Big|_{\varphi_0} = \frac{b}{a} \cot(\varphi_0) . \tag{6}$$

Sub-segment *TR* is a straight line that can be defined in a straightforward manner as

$$z - z_R = -\tan(\theta)(y - y_R), \qquad y \in [y_T, \quad y_R]. \tag{7}$$

where (y_R, z_R) and (y_T, z_T) are coordinates of points *T* and *R*, respectively.

Coordinates of point *R* are expressed differently at different types of offset in the weave. The variation of θ at all different offset scenarios is shown in Fig. 10 for a special case of $n_{deep}=n_{steep}=2$. This is nevertheless a pure geometric relationship referring to the overall configuration in Fig. 8 and the coordinates of point *R* are determined as summarised in Table 4.

The coordinates of point *T* can be obtained from Equation (5) at $\varphi = \varphi_0$, where angle φ_0 is associated with θ according to Equation (7). With coordinates of point *R* being defined, based on Equations (5) and (7), the relation between φ_0 and coordinates of *T* is established as

$$z\big|_{\varphi=\varphi_0} - z_R = -\frac{b}{a} \cot(\varphi_0) \left(y\big|_{\varphi=\varphi_0} - y_R \right), \tag{8}$$

Equation (8) defines a transcendental equation for φ_0. A closed-from solution is not usually attainable and one may have to resort to a numerical algorithm, e.g. the Newton's iteration scheme, to obtain a numerical solution. Once it is obtained, the position of point *T* can then be uniquely determined from Eq (5) with $\varphi = \varphi_0$. Equation (6) can be used to determine tan(θ) in a straightforward manner. This concludes the definition of segment *OSTR*.

Table 4 Coordinates of point *R* at different offset scenarios

Coordinate	n_{offset}=0	n_{offset}=-1	n_{offset}=1
y_R	$\frac{1}{2} n_{skip} \left(W_b + D_b\right)$	$n_{skip} \frac{W_b + D_b}{2}$	$\left(n_{skip} + n_{steep} - 1\right) \frac{W_b + D_b}{2}$
z_R	$-\frac{1}{2}\left(n_{steep} - 1\right)\left(H_a + H_b\right)$	$-\left(2n_{steep} - 1\right) \frac{H_a + H_b}{4}$	$-\frac{1}{2}\left(n_{steep} - 1\right)\left(H_a + H_b\right)$

For consistency of presentation, the ultimate set of parameters defining the tow geometry in a regular 3D weave is summarised in Table 5. Note that parameter D_a denoting the space between the adjacent warp tows has been referred to in the table. It was not involved in any derivations above, as it was unnecessary as far as geometric parametrisation is concerned. Furthermore, the gap between the warp tows is not always observed in the real composite. However, some spacing between the warp tows is desirable when generating the finite element model, as otherwise, the conformity of the mesh between the neighbouring warp tows would be difficult to keep. Likewise, if the spacing was too small, the quality of the mesh this area would be poor. As the spacing increases over a threshold, whilst easing the demand on meshing, noticeable deviation in the predicted results would be observed. The size of this gap has therefore been determined via a sensitivity study similar to mesh convergence study, where the gap value is reduced until there is little variation between predictions of the model.

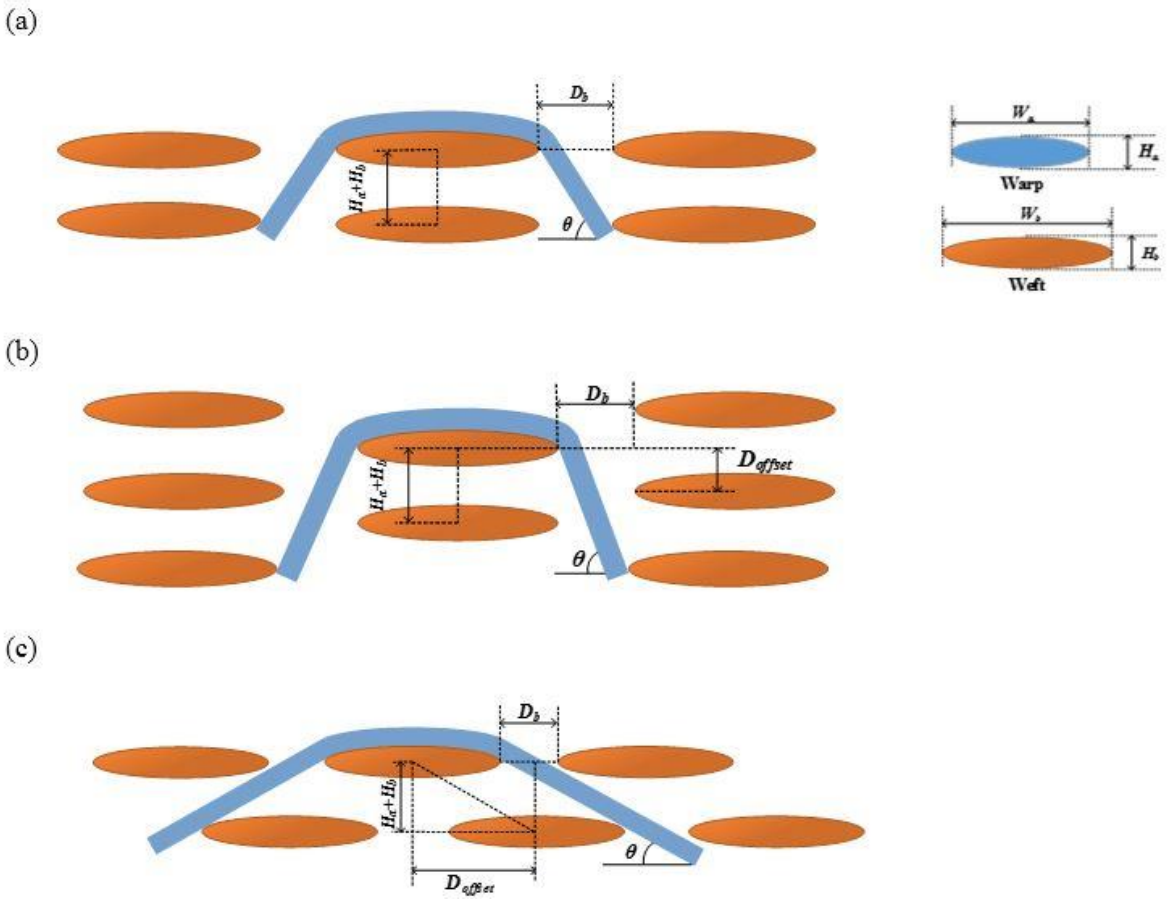

Fig. 10 Variation of θ for weaves of different topological parameter n_{offset}: (a) n_{offset}=0; (b) n_{offset}=1 with the distance of vertical offset being $D_{offset}=(H_a+H_b)/2$; (c) n_{offset}=1 with the distance of the horizontal offset being $D_{offset}=(W_b+D_b)/2$

Table 5 Parameters of the tow geometry.

Geometric feature of the tow	Warp	Weft
Thickness	W_a	W_b
Width	H_a	H_b
Shape parameter	γ_a	γ_b
Horizontal space between the adjacent tows	D_a	D_b

Once the base warp path (one-fourth of the full path in a period in Fig. 8) has been defined, the right part of the warp path along the thickness can be reproduced by the 180° rotation of the base warp path at point *R*. If the $n_{deep} = n_{steep}$, then the left half can be reproduced by mirror reflection at point *O*. If the $n_{deep} \neq n_{steep}$ (as illustrated in Fig. 4(c)),

segment *OSTRR'T'S'O'* will need to be rotated by 180° about point *O*. The process may have to be repeated $n_{deep}/n_{steep}-1$ times, if $n_{deep}/n_{steep}>2$ before mirror reflection is utilized.

Without loss of crucial information, the architecture within the UC can be idealised in such a way that it can be parameterised as elaborated above by using the available symmetries appropriately.

It should be noted that the tow path parametrisation was conducted under the assumption of weft tows being straight. This is reasonable for most 3D weaves, while in order to reproduce 2D weaves more realistically, the weft tows should be allowed to undulate same as the warp ones. Although not included here, the parametrisation methodology can be extended in a reasonably straightforward way to allow for such scenarios.

2.4 Unit cells for woven textile composites

The parametrisation as presented above helps to define the topology and the geometry of the weave architecture. The objective of the present exercise is to take the achievement a step further to formulate an appropriate unit cell which is fully parametrised and can be applied for numerical characterisation of woven textile composites.

The precondition for the definition of the UC is presence of translational symmetries in the material, as this is the only type of symmetry that reduces an infinite domain to a finite extent. Given the translational symmetries available in woven textile composites, the simplest shape for the UC in the base slice is apparently a cuboid.

With the periodicity in a base slice in both vertical and horizontal directions, a UC can be conveniently defined as a complete period of the slice in each of the two directions. In particular, a possible selection of a UC for the type of weave shown in Fig. 2(a) is marked by a red dashed rectangle. Mapping from one UC to another within a slice corresponds to a translation as a combination of these two orthogonal translations.

Mapping from a UC in one slice to that in another slice corresponds to a translation into or out of the page but non-orthogonal to the former two, as shown in Fig. 2, which is often present in structures of a staggered pattern [18] as sketched in Fig. 1. This allows to

reproduce other slices through the translational symmetry transformation of the base slices with the designated interlocking between the warp and weft tows duly represented.

Together, these three translations form a complete set of three-dimensional non-orthogonal translations through which the entire space of the 3D weave can be covered by the images of the UC under one of the translational symmetry transformations.

To complete the formulation of such UC, the boundary conditions for it should be derived. To do so, the methodology developed by Li et al. [16, 18, 22-25] has been followed that has a rigorous mathematical and mechanical background and offers great convenience in post-processing of the results. To avoid duplicating the derivations procedures, only the main aspects of the methodology are briefly outlined in this paper supported by references to relevant publications for interested readers to consult.

The boundary conditions are formulated based on the translational symmetries in terms of relative displacements, and for linear problems their general form is as follows [22]:

$$\left\{\begin{matrix} u \\ v \\ w \end{matrix}\right\}\Bigg|_{(x',y',z')} - \left\{\begin{matrix} u \\ v \\ w \end{matrix}\right\}\Bigg|_{(x,y.z)} = \boldsymbol{\varepsilon}^{\mathbf{0}}\Delta\mathbf{x} = \begin{bmatrix} \varepsilon_x^0 & 0 & 0 \\ \gamma_{xy}^0 & \varepsilon_y^0 & 0 \\ \gamma_{xz}^0 & \gamma_{yz}^0 & \varepsilon_z^0 \end{bmatrix} \left\{\begin{matrix} \Delta x \\ \Delta y \\ \Delta z \end{matrix}\right\}, \tag{9}$$

where $(u \quad v \quad w)^T$ are microscopic displacements, (x, y, z) and (x', y', z') the coordinates of the respective points on a pair of faces related through a translational symmetry; $\boldsymbol{\varepsilon}^{\mathbf{0}}$ is the average, or macroscopic, strain field. Components of vector $\Delta\mathbf{x}=[\Delta x \ \ \Delta y \ \ \Delta z]^T$ are calculated as the difference in coordinates between the corresponding points on the paired faces, namely:

$$\Delta\mathbf{x} = \left\{\begin{matrix} x'-x \\ y'-y \\ z'-z \end{matrix}\right\} \tag{10}$$

In case of a cuboidal UC that involves three orthogonal translations along the coordinate axes, three vectors $\Delta\mathbf{x}$ have to be defined, each corresponding to the respective translation [22]. Each will have only one non-zero component, corresponding to the dimension of the UC in the direction of translation. Defining UC based on orthogonal translations is an

approach preferred by many. However, it does not deliver the most efficient UC for woven composites in terms of its size and hence the computational costs. What is more important in the context of the present paper, such UCs cannot be easily unified trough parametrisation. Both of these drawbacks can be eliminated by considering a staggered arrangement of the UCs in *xy*-plane, as shown in Fig. 1. This makes the expression of the boundary conditions only a little more complicated, but these complications are outweighed by the gain.

The corresponding translational vectors and relative displacement boundary conditions for a cuboidal UC with staggered arrangement are summarised in Table 6. Note that these boundary conditions are to be applied on the faces of the UC. Those on the edges and the vertices will have to be imposed separately, to avoid procedural conflicts that may arise from presence of the redundant boundary conditions. The explicit expressions for boundary conditions on the edges and the vertices for staggered UCs can be found in [18].

Table 6 Relative displacement boundary conditions on the faces of a UC representing the woven textile composite

Directions	Vectors	Boundary conditions
ξ-axis	$\Delta\mathbf{x}_\eta = \begin{Bmatrix} W_{UC} \\ L_1 \\ 0 \end{Bmatrix}$	$\Delta\mathbf{u}_\eta = \begin{Bmatrix} u'-u \\ v'-v \\ w'-w \end{Bmatrix} = \begin{Bmatrix} W_{UC}\varepsilon_x^0 + L_1\gamma_{xy}^0 \\ L_1\varepsilon_y^0 \\ 0 \end{Bmatrix}$
η-axis	$\Delta\mathbf{x}_\xi = \begin{Bmatrix} W_{UC} \\ -L_2 \\ 0 \end{Bmatrix}$	$\Delta\mathbf{u}_\xi = \begin{Bmatrix} u'-u \\ v'-v \\ w'-w \end{Bmatrix} = \begin{Bmatrix} W_{UC}\varepsilon_x^0 - L_2\gamma_{xy}^0 \\ -L_2\varepsilon_y^0 \\ 0 \end{Bmatrix}$
y-axis	$\Delta\mathbf{x}_y = \begin{Bmatrix} 0 \\ L_{UC} \\ 0 \end{Bmatrix}$	$\Delta\mathbf{u}_y = \begin{Bmatrix} u'-u \\ v'-v \\ w'-w \end{Bmatrix} = \begin{Bmatrix} L_{UC}\gamma_{xy}^0 \\ L_{UC}\varepsilon_y^0 \\ 0 \end{Bmatrix}$
z-axis	$\Delta\mathbf{x}_z = \begin{Bmatrix} 0 \\ 0 \\ H_{UC} \end{Bmatrix}$	$\Delta\mathbf{u}_z = \begin{Bmatrix} u'-u \\ v'-v \\ w'-w \end{Bmatrix} = \begin{Bmatrix} H_{UC}\gamma_{xz}^0 \\ H_{UC}\gamma_{yz}^0 \\ H_{UC}\varepsilon_z^0 \end{Bmatrix}$

In the boundary conditions in Table 6, five more parameters are introduced. Three of them are the width, W_{UC}, the height, H_{UC}, and the length, L_{UC}, of the UC. Remaining two parameters, L_1 and L_2, are segments of L_{UC} associated with translations along η- and ξ-axis, respectively, and hence only one of them is independent. Their explicit expressions are as follows:

$$\begin{aligned} L_1 &= \frac{1}{2} n_{step} \left(W_a + D_a \right) \\ L_2 &= L_{UC} - L_{step1} \end{aligned} . \tag{11}$$

As can be seen, these parameters are expressed in terms of topological and geometric parameters introduced in the previous sections. Same is true for the actual dimensions of the UC as given in Table 7. Therefore, the imposition of the boundary conditions does not require specification of any further independent parameters.

Table 7 Parametrised dimensions of the UC at different types of offset

Type of offset	No offset/vertical offset	Horizontal offset
Dimensions of the UC	$W_{UC} = W_a + D_a$ $L_{UC} = 2n_{skip} \cdot \frac{n_{deep}}{n_{steep}} \left(W_b + D_b \right)$ $H_{UC} = H_a + H_b$	$W_{UC} = W_a + D_a$ $L_{UC} = \left(2n_{skip} + n_{deep} - 1 \right) \left(W_b + D_b \right)$ $H_{UC} = 2 \left(H_a + H_b \right)$

3 Implementation of parametrised 3D woven textile UCs

One of the major advantages of the parametrisation as presented in sections above is that it uses a fixed set of parameters that have a clear meaning and can be relatively easily defined for any weave type. It is true that their definition can vary in some cases, e.g. for different types of offset. However, these multiple choices can easily be automated by implementing the procedure as a computer code.

The parametrisation of textile composites as proposed above has been implemented on the platform of UnitCells© [26], which was a piece of software produced at the University of Nottingham as a secondary development of Abaqus CAE [27] specifically for analysis of

UCs of various types. It is essentially a code written in Python scripts, which incorporates various unit cells in a rigorous and systematic way according to their formulations and at the same time automates all the UC modelling steps, from generation of the geometry of an FE model to post-processing of the results to obtain effective properties. Though a range of UCs for certain types of textile composites has been incorporated in UnitCells©, their formulations have not been unified and such UCs have been defined based entirely on orthogonal translations. As has been explained earlier, unification has achieved via the employment of staggered translation and the parameterisation. It is timely to upgrade the code with the latest development.

UnitCells© has therefore been supplemented with a new UC parametrised as elaborated in previous sections, for which appropriate Python script was written. Part of this script, responsible for the generation of the FE model as well as conducting the analysis, was adapted from the existing UnitCells© [26] Python scripts. The results obtained as presented in the subsequent section of this paper were all produced using with this code.

4 Verification and validation of UC formulated

The parametrised UC implemented through the Python code has been subjected to "sanity checks" [22] to verify the correct application of the boundary conditions. To do so, the constituents of the UC were prescribed the same isotropic material properties and simple analysis was conducted to ensure that the uniform stress and displacement fields have been achieved under uniaxial direct and pure shear loadings. A range of different values of the topological and geometric parameters have been tested without any abnormal behaviour of the UC being observed. After passing this basic level of verification, the UC was subjected to the following validation against experimentally measured data available to the authors.

The UC of textile composite chosen for this purpose is shown in Fig. 11. It represents the 3D layer-to-layer angle interlock woven composite, the topology of which corresponds to parameter values as specified in Table 8. The geometric parameters of the tows, also specified in the same table, were measured from the micro-CT images given in [19]. The

properties of constituents, Gurit PRIME™ 20LV resin and IM7 carbon fibre tows, are summarised in Table 8. The properties of the latter were calculated conducting material characterisation in UnitCells©, where IM7 tows were considered as unidirectional composites at a micro-scale, for which fibre volume ratio (V_f) of 78.6% was assumed. With tow volume fraction in this particular model being 65.36%, the total fibre volume fraction is pragmatic 51.09%. The UC model was meshed with tetrahedral elements as shown in Fig. 11(a) for the fibre tows and (b) for the surrounding matrix, where the typical element size was 0.09 mm. The mesh was converged. Note that this mesh size is sufficient for the UC to characterise the effective elastic properties of the composite as addressed in this study, where the localised stress concentrations do not greatly affect the predictions. However, if one is interested in material strength, a more accurate stress distribution in stress concentration areas, where failure tends to initiate, will be essential and can be obtained with a more refined mesh.

The results of material characterisation are summarised in Table 9. Some of the material properties obtained have been compared with available experimental data reported in [15, 16], showing good agreement. In addition, the characterisation results reveal an interesting feature in mechanical behaviour of the given composite, namely, its tendency to expand in warp direction when stretched along the direction of weft tows. Numerically, it is expressed in terms of Poisson's ratio v_{xy} being negative. This kind of behaviour, which, to the best of the authors' knowledge has not yet been addressed experimentally, can be easily explained by observing the predicted deformation of the unit cell.

The deformation of unit cell loaded in the X-direction (weft) is shown Fig. 13(a), where it is magnified by the factor of 5×10^4 so that it could be clearly observed. Comparing the geometry of the deformed unit cell with the undeformed one in Fig. 13(b), it is easy to see that under the load, both the warp and the weft tows contract in Z-directions due to Poisson's effect. Fibre tows are very stiff in the axial direction and hence do not shrink much in their length. The warp tows have to rotate towards the warp direction to allow the Z-direction contraction of the unit cell, as indicated by red line and compared between both plots. The

fibre tow rotation impedes the sideways contraction of the unit cell and can even cause a marginal expansion. This effect would become less pronounced as axial Young's modulus reduces. This has been verified numerically analysing several cases where smaller values of axial Young's modulus were assigned. Note that the effect of negative Poisson's ratio is not a conventional experimental observation, and some might perceive such data to be erroneous. As has been shown here, careful assessment of properly devised model can easily dispel such misperception and extend the understanding of the mechanical behaviour of woven composites. With some more deliberate design, it is possible to obtain some auxetic materials through 3D woven composites.

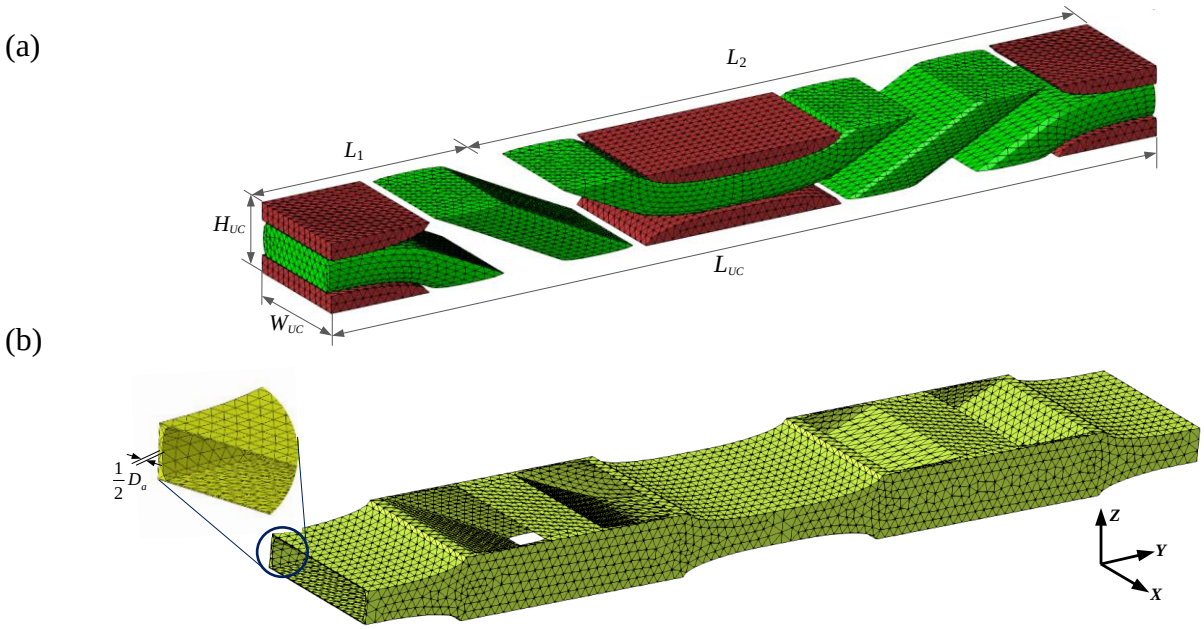

Fig. 11 Unit cell for the 3D interlocked woven architecture: the geometry and meshing of (a) the tows and (b) the matrix

Table 8 Input properties and parameters

Topological parameters		Geometric parameters			Material properties of constituents	
		Property	warp	weft	Matrix (PRIME™ 20LV) [28]	Tow (IM7 CF, V_f = 78.6%) [17]
n_{offset}	0	W (mm)	1.3	2.0	E=3.5 GPa	E_1=217.42GPa
n_{step}	1	H (mm)	0.3	0.27	v=0.35	E_2= E_3=12.21GPa
n_{skip}	1	γ	0.05	0.8	G=2.06 GPa	v_{12}=v_{13}=0.29
n_{deep}	2	D (mm)	0.05*	2.3		v_{23}=0.45

n_{steep}	2	G_{12}= G_{13}=5.29GPa G_{23} =4.21GPa

*Value of this parameter was determined from sensitivity study presented in Fig. 12

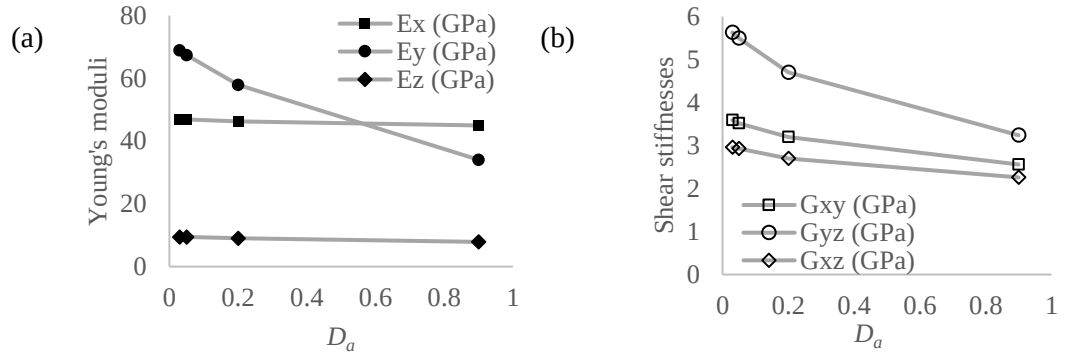

Fig. 12 Sensitivity studies to determine value of D_a: (a) variation of Young's moduli and (b) variation of shear stiffnesses

Table 9 Results from the unit cell of interlocked 3D woven textile

Architecture data		Properties		
			Simulation	Experiment [20]
Interlocking angle	21.96°	E_x (GPa)	46.91	45.00
Tow volume fraction	65.36%	E_y (GPa)	67.42	68.00
Fibre volume fraction	51.09%	E_z (GPa)	9.40	-
Weft/warp ratio	0.3873	ν_{xy}	-0.0016	
		ν_{xz}	0.4408	
		ν_{yz}	0.9721	
		G_{xy} (GPa)	3.52	3.62
		G_{xz} (GPa)	2.93	
		G_{yz} (GPa)	5.50	

This exercise demonstrates that the parametrised UC model is perfectly applicable for material characterisation, as was to be expected. It is worth noting that the UC model based on staggered arrangement is half the size of conventional UC model formulated based on orthogonal translations [17], as it incorporates only one set of warp tows, therefore, whilst having the same functionality, it substantially reduces the computational costs of the analysis.

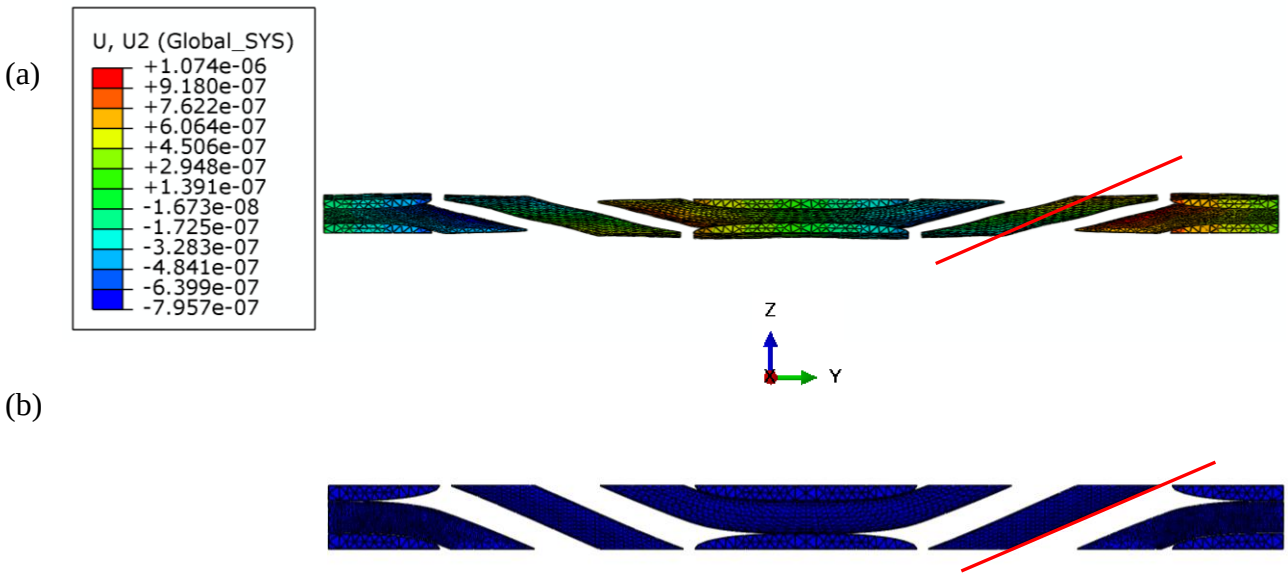

Fig. 13 Deformation of unit cell under weft tension (plot (a)) and undeformed reference geometry (plot (b))

5 Parametric studies of as an application of the UC formulated

With the UC fully established, an application of it has been made in this section to demonstrate the advantage of the parametrisation and its potential in supporting the design of 3D woven composites. A range of parametric studies has been devised, where one or more topological parameters vary while the rest are kept constant. The geometric parameters of the fibre tows as well as the material properties of constituents were kept constant as specified in Table 8.

In Fig. 14(b), the variation of the effective elastic material properties with parameter n_{step} increasing from 1 to 11 is shown. The UC model employed in this study is shown in Fig. 14(a). Variation of n_{step} does not alter the geometry of the UC but affects the relationship between the two slices, as it is involved in definition of staggered arrangement according to Eq. (10). Because of this, the interlocking angle of the warp tow, fibre volume fraction and weft/warp tow ratio stayed constant at 17°, 54.95% and 0.54, respectively, and the effective properties in the weft and through-thickness directions remained nearly the same at different

values of n_{step}. On the other hand, an apparent variation of the properties along warp direction, such as E_y, was predicted as n_{step} was varied. Note that the plots of variations of both E_y and G_{yz} are symmetric as n_{step} =1 and n_{step} =11 correspond to identical weave architectures.

(a)

(b)

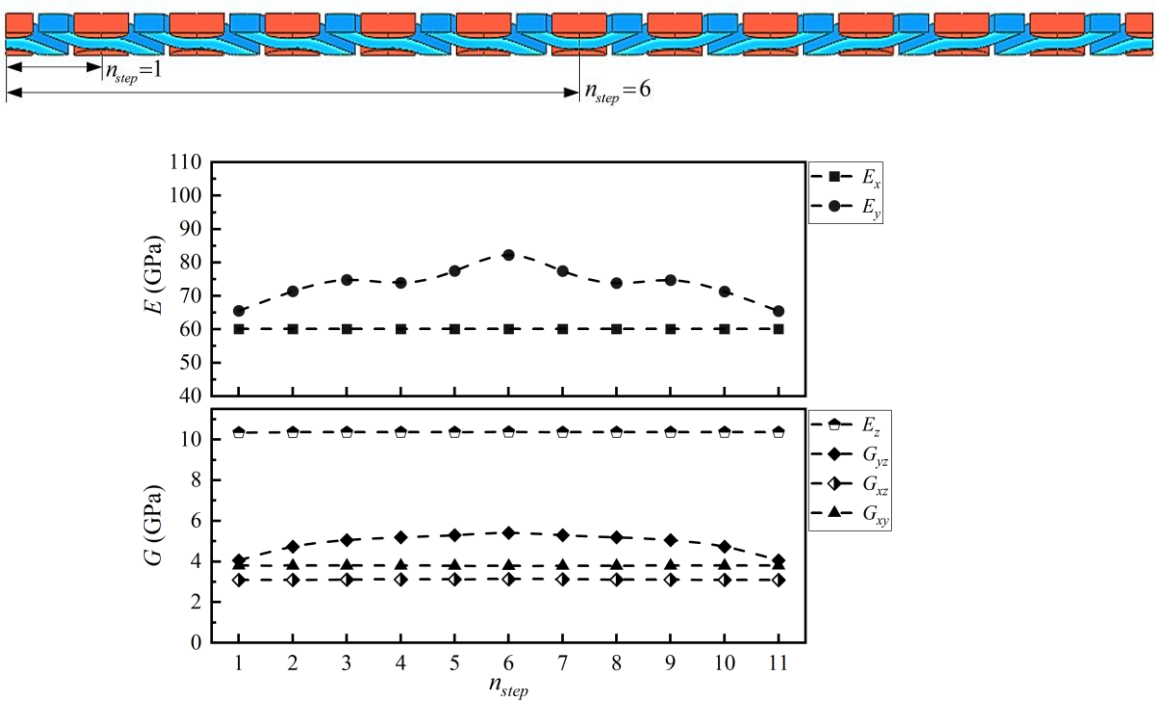

Fig. 14 Variation of parameter n_{step} at n_{offset}=0, n_{skip}=1, n_{deep}=6 and n_{steep}=1: (a) structure of UC; (b) effect of n_{step} on effective stiffnesses

More substantial warp stiffness variation can be observed in Fig. 15(b), where parameter n_{skip} was increasing from 1 to 7 in increments of 1, while the effective properties in the weft and through-thickness directions were generally unaffected, same as in previous case. The higher the value of n_{skip}, the straighter are the warp tows, as can be seen in the Fig. 15(a), where UC for n_{skip}=1 and n_{skip}=2 are shown. This explains the predicted increase in warp stiffness as can be seen in Fig. 15(b). Note that altering the topology of the weave had a substantial effect on geometry, specifically, the warp tow paths, which resulted in marginal variations of the total fibre volume fraction (V_f = 51.5%±0.2%) and weft/warp tow ratio (0.385). The interlocking angle of the warp tow has not been affected and kept constant at 21.9°.

(a)

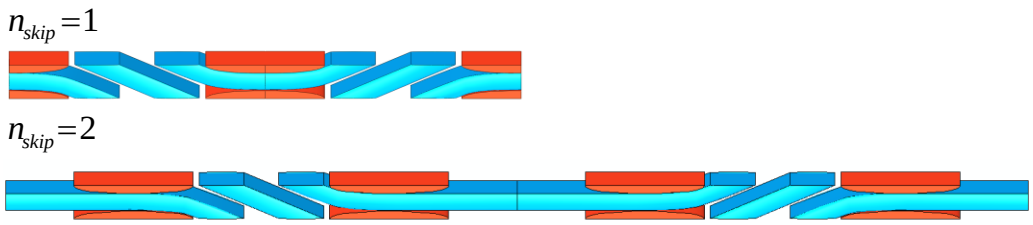

(b)

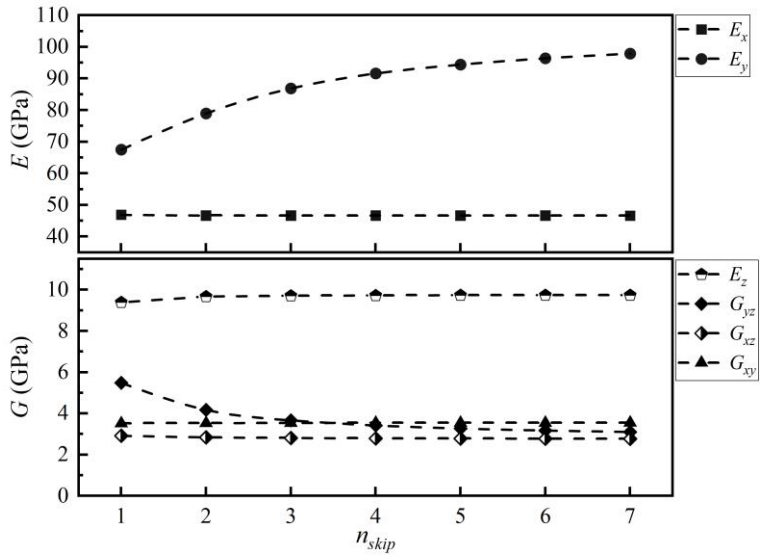

Fig. 15 Variation of parameter n_{skip} at n_{offset}=0, n_{step}=1, n_{deep}=2 and n_{steep}=2: (a) examples of UCs; (b) predicted variation of effective stiffnesses

Variation of n_{deep} extends the length of the UC but does not substantially alter the geometry, as can be seen in Fig. 16(a), where the two UCs shown maintained the same interlocking angle of 10°. Consequently, little or no variation of effective elastic properties was predicted in this case, as shown in Fig. 16(b). The total fibre volume fraction and weft/warp tow ratio kept nearly the same at around 49.8% and 0.40, respectively.

(a)

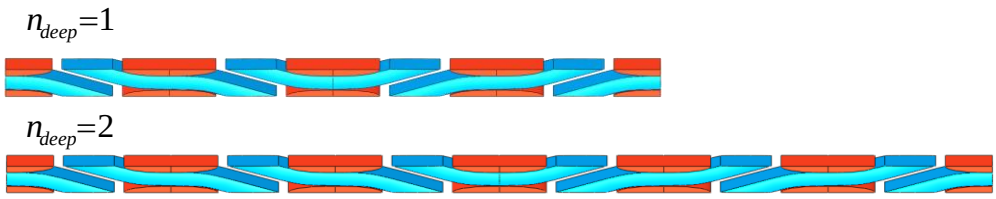

(b)

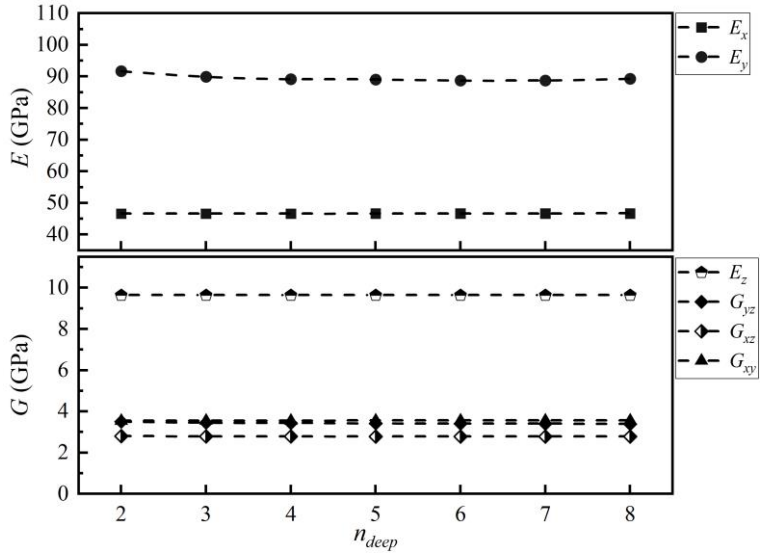

Fig. 16 Variation of n_{deep} at n_{offset}=0, n_{step}=1, n_{skip}=1 and n_{steep}=1: (a) typical examples of UCs; (b) predicted variation of effective stiffness properties

Unlike in the previous case, the warp weaving angle changed substantially when parameter n_{steep} was altered, as can be seen in Fig. 17(a). Note that in this case, the gap D_b between the weft tows had to be manually enlarged, with its values being given Fig. 17(b), to allow multiple warp tows pass through the gap and to maintain similar fibre volume fraction of V_f = 55.3%±0.3% for all the UCs. As can be seen in Fig. 17(b), the interlocking angle increased with n_{steep}, which resulted in rapid reduction of predicted E_y from 68 MPa at n_{steep}=1 to 20 MPa at n_{steep}=6 (Fig. 17(c)). However, the increase of n_{steep} is advantageous in terms of through the thickness stiffness. The increase of D_b is accompanied by reduction of the weft/warp tow ratio, which is also plotted Fig. 17(b).With smaller portion of weft tows, the reduction in weft stiffness E_x can naturally be expected, and this is indeed the case for the predicted values of E_x in Fig. 17(c).

(a)

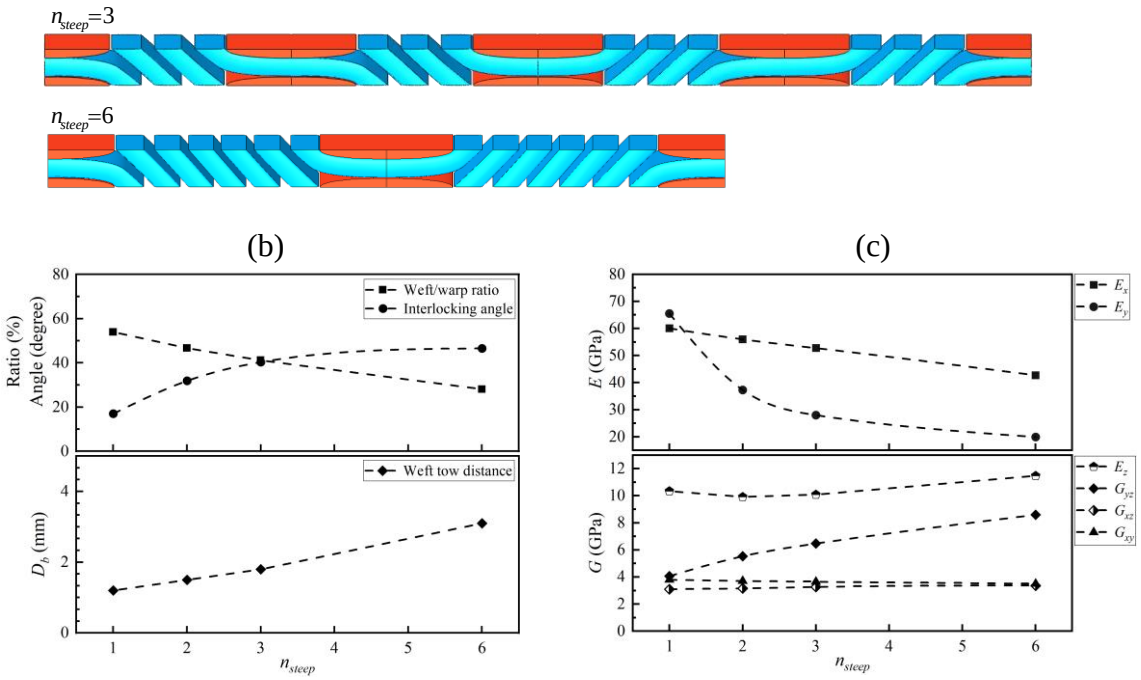

Fig. 17 Variation of n_{steep} at n_{offset}=0, n_{step}=1 and n_{skip}=1, n_{deep}=6: (a) typical UCs; (b) variation of geometry; (c) predicted variation of effective stiffnesses

6 Conclusions

The design tool for 3D woven textile composites has been developed. As the main outcome of this paper, unified definition of a wide range of 2D and 3D weaves has been achieved via a comprehensive parametrisation of the weave by taking advantage of translational symmetries along non-orthogonal directions. This is different from conventional selection of UC for textile composites, which typically involve orthogonal translations in three directions. As an added significant advantage, the former method is more computationally effective as compared to the latter case.

With the UC modelling being the dominant approach to numerical characterisation of textile composites, the parametrisation as developed here is perfectly suited for generation of FE models of UCs.

Thirteen parameters were found to be sufficient for the purpose. Five of them are topological parameters of a simple meaning that can interpreted as explained in Section 2.1. The remaining eight are the geometric parameters, seven of which are conventionally

employed in modelling of textile composites, and one is introduced for convenience in meshing and it does not significantly affect the predicted properties.

The parameterisation was incorporated into the FE modelling by combining it with an earlier development, a piece of software for material characterisation called UnitCells©. This completes the development of the design tool. The development has been verified and validated against limited experimental data available.

As an example of application of the capability developed, the variations of effective properties with respect to the variations of the topology of the weaves have been shown through a number of case studies, where material characterisations have been carried out while varying the topological parameters. This demonstrates the potential of the parametrised UC for 2D/3D woven composites in numerical characterisations of such composites, which could be turned into an efficient design tool for such composites.

Acknowledgement

The authors would like to thank AECC CAE, China contract number 126961 for providing financial support for this research. The first author wishes to acknowledge the scholarship from CSC, China and the Faculty of Engineering, the University of Nottingham, UK.

References

1. Mouritz AP, Bannister MK, Falzon PJ, Leong KH. Review of applications for advanced three-dimensional fibre textile composites. Composites Part A: Applied Science and Manufacturing, 1999. **30**(12):1445-1461.
2. Dai S, Cunningham PR, Marshall S, Silva C. Influence of fibre architecture on the tensile, compressive and flexural behaviour of 3D woven composites. Composites Part A: Applied Science and Manufacturing, 2015. **69**:195-207.
3. Leong KH, Lee B, Herszberg I, Bannister MK. The effect of binder path on the tensile properties and failure of multilayer woven CFRP composites. Composites Science and Technology, 2000. **60**(1):149-156.
4. Hale RD. An experimental investigation into strain distribution in 2D and 3D textile composites. Composites Science and Technology, 2003. **63**(15):2171-2185.
5. Saleh MN, Soutis C. Recent advancements in mechanical characterisation of 3D woven composites. Mechanics of Advanced Materials and Modern Processes, 2017. **3**(1):12.

6. Tarnopol'skii YM, Kulakov VL, Aranautov AK. Measurements of shear characteristics of textile composites. Computers & Structures, 2000. **76**(1):115-123.
7. Ansar M, Wang X, Zhou C. Modeling strategies of 3D woven composites: A review. Composite Structures, 2011. **93**(8):1947-1963.
8. Green SD, Matveev MY, Long AC, Ivanov D, Hallett SR. Mechanical modelling of 3D woven composites considering realistic unit cell geometry. Composite Structures, 2014. **118**:284-293.
9. Liu LL, Xuan HJ, Chen W, Zhao ZH, Guan YP, He MH. Modified Subcell Model Using Solid Elements for Triaxial Braided Composite under Ballistic Impact. Journal of Aerospace Engineering, 2016. **29**(5).
10. Gereke T, Cherif C. A review of numerical models for 3D woven composite reinforcements. Composite Structures, 2019. **209**:60-66.
11. Boussu F, Cristian I, Nauman S. General definition of 3D warp interlock fabric architecture. Composites Part B-Engineering, 2015. **81**:171-188.
12. Chen X, Potiyaraj P. CAD/CAM of orthogonal and angle-interlock woven structures for industrial applications. Textile Research Journal, 1999. **69**(9):648-655.
13. Adanur S, Liao TY. 3D modeling of textile composite preforms. Composites Part B-Engineering, 1998. **29**(6):787-793.
14. Wang XF, Wang XW, Zhou GM, Zhou CW. Multi-scale Analyses of 3D Woven Composite Based On Periodicity Boundary Conditions. Journal of Composite Materials, 2007. **41**(14):1773-1788.
15. Ha MH, Cauvin L, Rassineux A. A methodology to mesh mesoscopic representative volume element of 3D interlock woven composites impregnated with resin. Comptes Rendus Mécanique, 2016. **344**(4-5):267-283.
16. Li S, Zhou C, Yu H, Li L. Formulation of a unit cell of a reduced size for plain weave textile composites. Computational Materials Science, 2011. **50**(5):1770-1780.
17. Pan Q. Multi-scale modelling and material characterisation of textile composites for aerospace applications. 2016, University of Nottingham.
18. Li S, Warrior N, Zou Z, Almaskari F. A unit cell for FE analysis of materials with the microstructure of a staggered pattern. Composites Part a-Applied Science and Manufacturing, 2011. **42**(7):801-811.
19. Yu T. Continuum damage mechanics models and their applications to composite components of aero-engines. 2016, University of Nottingham.
20. Kong W. Macro-scale modelling of the impact response of 3D woven composites for aerospace applications. 2016, University of Nottingham.
21. Teply JL, Dvorak GL. Bounds on overall instantaneous properties of elastic-plastic composites. Journal of the Mechanics and Physics of Solids, 1998. **36**:29-58.
22. Li S, Sitnikova E. *1.18 An Excursion into Representative Volume Elements and Unit Cells*, in *Comprehensive Composite Materials II*. 2018, Elsevier: Oxford. p. 451-489.
23. Li S, Singh CV, Talreja R. A representative volume element based on translational symmetries for FE analysis of cracked laminates with two arrays of cracks. International Journal of Solids and Structures, 2009. **46**(7):1793-1804.
24. Li SG. Boundary conditions for unit cells from periodic microstructures and their implications. Composites Science and Technology, 2008. **68**(9):1962-1974.
25. Li S. General unit cells for micromechanical analyses of unidirectional composites. Composites Part A-Applied Science and Manufacturing, 2001. **32**(6):815-826.
26. Li S, Jeanmeure LFC, Pan Q. A composite material characterisation tool: UnitCells. Journal of Engineering Mathematics, 2015. **95**(1):279-293.
27. Abaqus GUI Toolkit User's Guide, Abaqus/CAE 2018, Dassault Systèmes© A.f.U.o. Nottingham, Editor. 2018.

28. DATASHEET / PRIME™ 20LV - Epoxy Infusion System (v13), Gurit©, Editor. 2019.